Journal of Materials Chemistry C

PAPER

Check for updates

Highly conductive and long-term stable films from liquid-phase exfoliated platinum diselenide†

Kangho Lee, [ID] [a] Beata M. Szydłowska, [ID] [ab] Oliver Hartwig, [ID] [a]
Kevin Synnatschke, [ID] [c] Bartlomiej Tywoniuk, [ID] [a] Tomáš Hartman, [d]
Tijana Tomašević-Ilić, [e] Cian P. Gabbett, [c] Jonathan N. Coleman, [ID] [c]
Zdeněk Sofer, [ID] [d] Marko Spasenović, [ID] [f] Claudia Backes [ID] [bg] and
Georg S. Duesberg [ID] *[a]

Liquid-phase exfoliation (LPE) has been introduced as a versatile and scalable production method for two-dimensional (2D) materials. This method yields dispersions that allow for the fabrication of printable and flexible electronic devices. However, the fabrication of uniform and homogeneous films from LPE dispersions with a performance similar to that of bottom-up grown materials remains a challenge, as the film quality strongly influences the optical and electrical performance of devices. Furthermore, long-term stability remains a major challenge for all 2D material based applications. In this study, we report on highly conductive tiled network films made of platinum diselenide ($PtSe_2$) flakes derived using a scalable LPE method. We characterized the homogeneous films in terms of morphology and electrical behavior. As an example of applicability, we produce a chemiresistive sensor structure with the $PtSe_2$ films and show significant resistance changes upon periodic ammonia gas exposures, revealing a sub-0.1 part per million (ppm) detection limit (DL). More remarkably the devices are fully functional after 15 months, underlining the high stability of $PtSe_2$ based devices.

Introduction

The unique properties of two-dimensional (2D) materials that enable high potential for their employment in numerous applications have led to enormous scientific interest.[1–3] In particular, they have been proposed for chemical sensing due to their high surface-area-to-volume ratio. Graphene-based sensors have shown ultimate sensitivity, detecting even individual gas molecules[4] while 2D transition metal dichalcogenide (TMD) materials showed extreme sensitivities to trace gases.[5–13] In particular, $PtSe_2$ has been shown to have superior gas sensitivity,[11] and gas selectivity was predicted by density functional theory.[14] Moreover, the outstanding electrochemical properties of platinum chalcogen compounds show promise for further applications.[15,16]

Within the toolset for the production of these materials, liquid phase exfoliation (LPE) has been proposed as a means for achieving high volume and yield. LPE has been used to exfoliate a range of 2D materials including graphite,[17–22] boron nitride,[23,24] pnictogens,[25–30] TMDs,[24,31–37] III–V semiconductors,[38] metal oxides,[39–41] and many others.[42–47] LPE is used to produce 2D materials in liquid dispersions, which can be used as inks, making the method attractive for various printing technologies, which allow for the fabrication of flexible devices or back end of line (BEOL) integration with existing integrated chips.[24,48] Most recently we were able to report on LPE-$PtSe_2$.[49]

Methods for producing films from LPE materials include vacuum filtration,[17,19] Langmuir–Blodgett (LB) deposition,[50–54] spray-coating[55] and inkjet printing.[56] However, many of these methods suffer from flake reaggregation into clusters in solution and on the substrate, leading to inhomogeneous films. In order to compensate for this, extra layers of materials must be added resulting in thick films ($>1\ \mu m$) which is detrimental

[a] *Institute of Physics, EIT 2, Faculty of Electrical Engineering and Information Technology, University of the Bundeswehr Munich & SENS Research Center, Werner-Heisenberg-Weg 39, 85577, Neubiberg, Germany. E-mail: duesberg@unibw.de*

[b] *Institute of Physical Chemistry, Heidelberg University, 69120, Heidelberg, Germany*

[c] *School of Physics, CRANN & AMBER Research Centres, Trinity College Dublin, Dublin 2, Ireland*

[d] *Department of Inorganic Chemistry, University of Chemistry and Technology Prague, Technicka 5, 166 28, Prague 6, Czech Republic*

[e] *Institute of Physics Belgrade, University of Belgrade, Pregrevica 118, 11080, Belgrade, Serbia*

[f] *Center for Microelectronic Technologies, Institute of Chemistry, Technology and Metallurgy, University of Belgrade, Njegoševa 12, 11000, Belgrade, Serbia*

[g] *Physical Chemistry of Nanomaterials, University of Kassel, Heinrich-Plett-Str. 40, 34132, Kassel, Germany*

† Electronic supplementary information (ESI) available: Additional comparison of LB-type nanosheet networks. See DOI: https://doi.org/10.1039/d2tc03889g

This journal is © The Royal Society of Chemistry 2023

J. Mater. Chem. C, 2023, 11, 593–599 | 593

in numerous applications and significantly increases production costs. Therefore, the formation of very thin homogenous films from LPE materials is not only crucial to the electrical and optical performance of devices, but is also a determining factor in the applicability of production methods.

Here we report for the first time film formation from $PtSe_2$ dispersions using a modified LB method at a liquid–liquid interface. Homogeneous films with low roughness and controllable thickness could be produced. These films were characterized using Raman spectroscopy, atomic force microscopy (AFM), and scanning electron microscopy (SEM) and compared to the conventional spray-deposited films. We contacted the LB films with interdigitated electrodes for electrical characterization. In a simple chemiresistive sensor structure, we show high sensitivity and fast response upon exposure to ammonia (NH_3) gas. Notably, we demonstrate the long-term stability of our films over 15 months.

Experimental

Synthesis of bulk crystals

Platinum sponge (Pt 99.99%, Surepure Chemetals) and selenium (Se 99.9999%, granules 2–4 mm, Wuhan Xinrong New Materials Co.) were placed in a quartz ampoule and sealed by an oxygen–hydrogen welding torch at a pressure of 1 mPa. Selenium was used in 2 at% excess. The ampoule was heated at 1270 °C in a 5 °C per minute of ramping speed and cooled down to 1000 °C at a 1 °C per minute of cooling rate after 30 minutes of dwell time. Afterwards, it was completely cooled down to room temperature. The selenium excess condensed on the opposite side of the ampoule, and the formed crystalline block of $PtSe_2$ was removed from the ampoule.

Preparation of the dispersions

The $PtSe_2$ dispersions were prepared using our previously established methodology of tip sonication and size selection by centrifugation in aqueous sodium cholate solution[57] followed by transfer to N-methyl-2-pyrrolidone (NMP) to aid the deposition at the liquid–liquid interface. $PtSe_2$ crystals were ground and immersed in 35 mL of aqueous sodium cholate (SC) solution (concentrations: $C_{PtSe_2} = 0.5$ g L^{-1} and $C_{SC} = 1.7$ g L^{-1}) and ultrasonicated (Sonics VXC500, 500 W, equipped with a tapered microtip) for 7.5 hours at 30% amplitude with a pulse of 6 seconds on and 4 seconds off. The dispersion was kept in a 4 °C cooling cell during sonication to avoid heating. The polydispersity of the as-produced dispersion was reduced by two consecutive centrifugation runs. High mass nanosheets which are larger and simultaneously thicker were discarded as sediment after the first run at lower centrifugal acceleration, while smaller/thinner nanosheets were removed as the supernatant after the second step at higher centrifugal acceleration. Specifically, unless otherwise noted, centrifugation was performed in a Hettich Mikro 220R centrifuge for 2 hours at 13 °C. The first step at a relative centrifugal force of 3000g (where g denotes the earth's gravitational field) was carried out with a fixed-angle rotor 1016 in

50 mL centrifuge tubes filled with $\sim$17 mL each. The supernatant was decanted and subjected to a second centrifugation at 5000g (with a fixed-angle rotor 1995-A in 1.5 mL Eppendorf tubes) after which the sediment was collected in deionized (DI) water and the supernatant discarded.

Preparation of films

Films were deposited after pre-assembly of the nanosheets at the liquid–liquid interface. First, the aqueous dispersion was transferred to NMP. To this end, the dispersion was centrifuged at 6000g (2 hours) to force the nanosheets to sediment and the sediment was redispersed in isopropanol (IPA) by bath-sonication for 5 minutes. The aqueous supernatant containing mostly water/surfactant was discarded. The centrifugation was repeated, the supernatant containing residual water and IPA was discarded and the sediment redispersed in NMP by 5 minutes of bath sonication. As substrates, SiO_2/Si wafers were chosen with an oxide thickness of 300 nm. These were diced to a size of 15 by 7.5 mm^2, cleaned by bath sonication in acetone, IPA, ethanol, and water for 20 min in each solvent and subsequently dried under a stream of pressured nitrogen. Fig. 1 depicts a schematic of the controlled deposition of $PtSe_2$ nanosheets on a SiO_2/Si substrate. Overall, the procedure can be regarded as a LB type deposition using two immiscible solvents, in this case water and toluene. It has been demonstrated that nanoflakes can be trapped at the liquid–liquid interface when injecting the LPE dispersion at an angle close to 90° with respect to the interface.[58,59] To form the liquid–liquid interface, first, a 15 mL glass beaker was filled with 12 mL of DI water and 0.5 mL of toluene was layered on top. Next, 0.1 mL of the $PtSe_2$ dispersion in NMP were gently injected on top and allowed to rest for 3 minutes to allow diffusion of the nanosheets to the toluene/water interface. After a uniform layer was formed, the toluene was allowed to evaporate and subsequently the transfer to the substrate was performed. To this end, the substrate was vertically introduced into the water phase, then tilted to an angle near 90° relative to the interface and then lifted up manually with a tweezer at speeds as constant as possible.[60] Generally, a smaller angle between the substrate and film is more favorable for the film transfer. Finally, the film was left to dry in air for $\sim$15 min with a tilt angle of $\sim$30° before performing a washing step by rinsing the films gently with a 1:1 mixture of IPA and DI water. Excess of unnecessary film
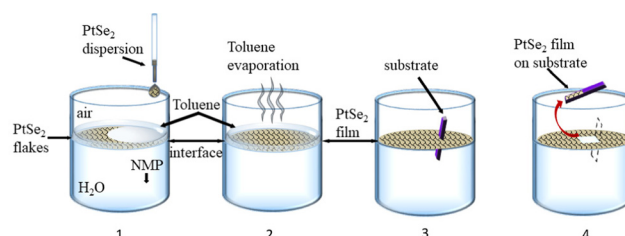

Fig. 1 Schematic of the modified Langmuir−Blodgett method to produce tiled nanosheet networks after pre-assembly at a liquid−liquid interface (1-film formation, 2-interface area reduction by evaporation, 3-substrate immersion, and 4-film deposition).

594 | J. Mater. Chem. C, 2023, 11, 593–599

This journal is © The Royal Society of Chemistry 2023

area was removed by gently scraping with a cotton swab, leaving an area of approximately 5 by 5 mm^2 in the center of the substrate.

Characterization

Scanning electron microscopy (SEM) characterization was performed with a JEOL JSM-6700F field emission SEM at 1 kV of acceleration voltage. Raman characterization was performed by mapping a region of 50 by 50 μm^2 with 100 measurement spots with a Witec alpha300 R confocal Raman microscope at an excitation wavelength of 532 nm at 0.5 mW of LASER power. For atomic force microscopy (AFM) imaging, a Dimension ICON3 scanning probe microscope (Bruker AXS S.A.S.) was used in ScanAsyst mode (non-contact) in air under ambient conditions using aluminium coated silicon cantilevers (OLTESPA-R3). Typical image sizes were 3 by 3 μm^2 scanned with 1024 lines at scan rates of ~ 0.4 Hz.

Device fabrication and measurement

Electrical characterization was performed in a Suss probestation using a SourceMeter$^{\circledR}$ Unit (Keithley model 2612A) at a scan rate of 10 mV s^{-1}. For gas sensor tests, interdigitated electrodes (Ni/Au = 40/45 nm) forming a 200 μm channel with a channel length-to-width ratio 1 : 277 were deposited on top of the films through a metal shadow mask. The PtSe$_2$ sensors were annealed for 2 hours at 150 °C in N$_2$ at ambient pressure to desorb attached gaseous molecules on the surface and then loaded into a custom-made sensing chamber. The annealing temperature was kept low in order to avoid changes in morphology that were cautioned against in work previously reported.[61] The sensing chamber pressure is kept at approximately 900 mbar by constantly flowing 100 standard cubic centimeters per minute (sccm) of gas through the chamber. The gas concentration is remotely controlled through a flow rate ratio modulation between dry N$_2$ and 10 part per million (ppm) of NH$_3$ gas. A SourceMeter$^{\circledR}$ Unit (Keithley model 2636B) monitors current changes upon periodic NH$_3$ gas exposure at a constant voltage bias.

Results and discussion

A liquid–liquid interface is created by layering toluene on top of water. The PtSe$_2$-NMP dispersion was added to the interface in a similar way as demonstrated earlier for LB graphene films at a water–air interface.[53,54,62] The interfacial tension at the toluene–water interface exerts surface pressure that compresses the interfacial nanosheets into a close-packed structure.[63] The substrate coverage can be controlled by adjusting the concentration of flakes in the solution and the interfacial area between the two phases. In this case, the optimum PtSe$_2$ concentration was found by trial and error.

After drying (see the Experimental section), SEM (Fig. 2a) and AFM (Fig. 2b) of the LB film reveal that it consists of a homogenous nanosheet network over large areas. The films appear continuous with feature sizes, typically <100 nm. The AFM measurement reveals a root-mean square (RMS) roughness of
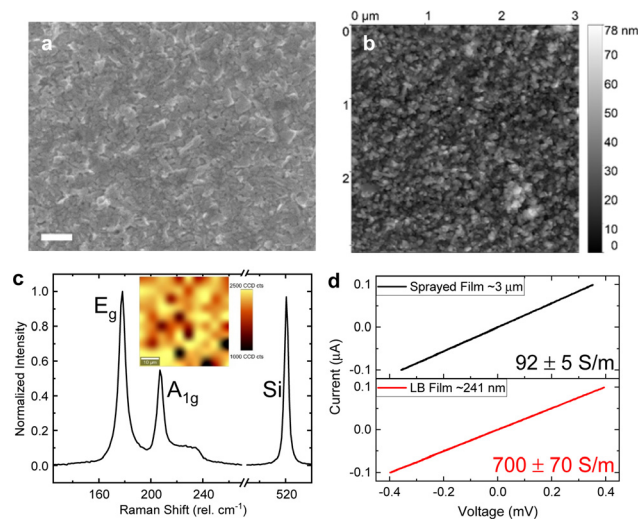

Fig. 2 (a) SEM image (scale bar: 200 nm) showing good nanosheet alignment and (b) AFM image of the LPE–PtSe$_2$ LB film. (c) Averaged Raman spectrum of the LPE–PtSe$_2$ LB film. Inset: scanning Raman map of the E$_g$ peak sum over a 50 by 50 μm^2 area. (d) Current–voltage characteristics of conventional spray-deposited and LPE–LB deposited films, resulting in film conductivities of 92 ± 5 and 700 ± 70 S m^{-1}, respectively. Note that the film thickness of the LB film (~ 240 nm) is more than 12-fold thinner compared to the sprayed network (~ 3 μm).

8.2 nm with only a few gaps between the sheets that are otherwise homogeneously deposited with maximum edge–edge contact. A scan at the edge of the film revealed a film thickness of ~ 30 nm (see the ESI†). Thus, one can conclude that thin films from platelets of PtSe$_2$ have been produced.

An averaged Raman spectrum from 100 positions on a sample is shown in Fig. 2c. Two prominent peaks can be identified at 178 and 207 cm^{-1}, which correspond to the in-plane E$_g$ and out-of-plane A$_{1g}$ vibrational Raman active modes, respectively. The inset depicts the spatial distribution of the E$_g$ mode at a location on the sample from which the averaged spectrum was measured. The Raman spectra contain well-defined, relatively narrow modes suggesting intact, crystalline nanosheets are deposited. Using our previously established quantitative metric for the estimation of PtSe$_2$ nanosheet thickness from Raman spectroscopy,[57] we estimate an average layer number of the nanosheets of 5.5. In previous work, we also established a correlation between the nanosheet layer number and lateral size,[57,64] which allows us to infer the average lateral dimensions of the nanosheets as ~ 60 nm (across the longest dimension) which is consistent with the microscopic characterization described above.

This modified LB film production method promises a higher conductive tiled network structure in comparison to randomly restacked porous nanosheet films produced by conventional spray deposition. To confirm this, another set of films were produced to allow for a direct comparison of LB-type and sprayed PtSe$_2$ networks, respectively. Due to the relatively high mass required for spray deposition, a more polydisperse PtSe$_2$ dispersion was used that was produced from centrifugation with a wider spread in the centrifugation boundaries (400g in the first step and 30 000g in the second step). Note that this resulted in a

This journal is © The Royal Society of Chemistry 2023

J. Mater. Chem. C, 2023, 11, 593–599 | 595

more polydisperse size distribution and thicker, rougher films compared to the production method used for the remainder of the work (see the ESI†). Therefore, it was required to perform two subsequent deposition cycles in the case of this sample to yield a continuous network. While the more than 12 times thicker, ~ 3 μm thick sprayed $PtSe_2$ film (Fig. S2a, ESI†) showed a conductivity of 92 ± 5 S m^{-1}, the ~ 240 nm thick $PtSe_2$-LB film (Fig. S2c, ESI†) showed approximately 7.6 times higher conductivity, 700 ± 70 S m^{-1} in 4-point probe measurements as shown in Fig. 2d. This is a result tentatively assigned to the better alignment of $PtSe_2$ nanoflakes in the modified LB films. As a result, the modified LB film yields generally much thinner films with good conductivity. On the one hand, this reduces the material mass required for 2D material nanosheet network structures which is an important aspect for $PtSe_2$ containing a precious metal. On the other hand, this can be beneficial for sensing applications due to better accessibility of the active material.

Fig. 3a depicts the current–voltage (I_{ds}–V_{ds}) curves measured on a sensor device where the film shown in Fig. 2a–c was contacted with interdigitated electrodes (inset) directly after fabrication and after 15 months. The slope of the curve yields a resistance of 61.8 kΩ for this device which corresponds to a conductivity of ~ 1.95 S m^{-1} in this device structure. The lower conductivity of this 30 nm thin film compared to the 240 nm thick LB-type film (Fig. 2d) can be rationalized by a different nanosheet size distribution and hence different junction resistance, as well as a different device structure. The high resistance indicates lower conductivity than $PtSe_2$ films grown by chemical vapour deposition[11,65–67] which may be attributed to flake-to-flake junctions hampering charge carrier transport.[52,68,69]

The contacted films were tested as ammonia sensors immediately after preparation and 15 months later to test the long-term stability of the device. Since many 2D materials, including group VI transition metal dichalcogenides,[70] are prone to degradation, for example by exposure to ambient conditions, we placed particular emphasis on the long-term stability of the sensor, as nanosheet degradation can cause inferior device performance. The device was tested as a gas sensor by exposing it to various concentrations of NH_3 in N_2 (0.1 to 0.8 ppm). The analyte was periodically introduced for 1 minute at a fixed concentration and at room temperature, followed by introduction of dry N_2 for 5 minutes for sensor recovery. No further treatments to enhance the recovery speed, *e.g.*, ultraviolet light illumination or annealing at higher temperatures, were applied. At 5 V of bias voltage, real-time current changes of the structured LPE-$PtSe_2$ LB film sensor can be calculated,

$$S = \frac{R_S - R_0}{R_0} \times 100\%$$

where R_0 and R_S are the resistances of the sensor before and after gas introduction. Fig. 3b shows a typical relative percentile resistance change as sensor responses. The resistance of the sensor increases upon NH_3 exposure because $PtSe_2$ is known as a p-type material and NH_3 donates an electron which results in reduction of the majority carrier in the semiconducting channel. To verify the sensor responses, simple signal processing was used.[7,11,71] The initial sensor resistance is calculated from the first 200 data points just before the first gas introduction. In the same regime, the root-mean-square (RMS) noise for a measured R_S is derived from the initial sensor resistance,

$$\text{Noise}_{\text{RMS}} = \sqrt{\sum \frac{(R_S - R_{\text{Base}})^2}{N}}$$

where R_{Base} is the baseline of the initial sensor resistance, and N is the number of data points. The signal-to-noise ratios (SNRs) derived from the resistance increments at various NH_3 concentrations are proportional to the gas concentration which is well-fitted to an exponential decay curve as shown in Fig. 3c. To be a true signal, the SNR must be at least three times larger or more according to the International Union of Pure and Applied Chemistry (IUPAC) definition.[72] In our measurements, an SNR of 3.4 was obtained for a concentration of 0.1 ppm of NH_3, setting a detection limit for this gas with LPE-$PtSe_2$ LB film sensors. In the SNR changes depicted at various concentrations (Fig. 3c), one can determine a theoretical detection limit (DL) by extrapolation to the point where the SNR drops below 3. This theoretical DL reaches a value of only 0.059 ppm, which is remarkable, as detection of low concentrations of NH_3 is challenging in chemiresistors because little charge is transferred compared to other analytes. This DL is one of the lowest values reported for LPE derived 2D material based gas sensors.[14,73,74]
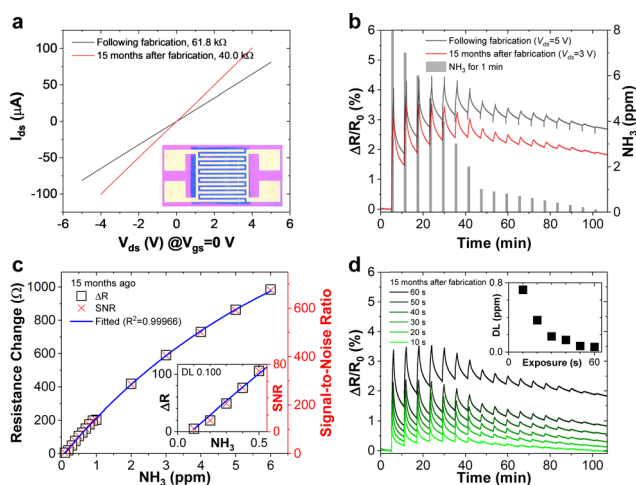

Fig. 3 (a) Current–voltage (I_{ds}–V_{ds}) characteristics of an LPE-$PtSe_2$ LB film sensor showing a noticeable conductance change after long-term exposure to the atmosphere. Inset: photograph of an LPE-$PtSe_2$ LB film (blue area) underneath interdigitated electrodes. (b) Sensor response curves of the LPE-$PtSe_2$ LB film sensor upon introduction of periodically decreasing concentrations of NH_3 from 8 down to 0.1 ppm (gray columns) at room temperature. A NH_3 sensor response is still observed 15 months later. (c) Resistance (open boxes) and SNR (red x-crosses) changes are proportional to the introduced gas concentration. Inset: zoomed-in plot in the lower NH_3 concentration range. (d) Sensor response curves for 10 to 60 seconds of NH_3 gas introduction (from light green to dark green). Inset: detectable NH_3 gas concentration inversely decreases as the gas exposure time increases.

596 | *J. Mater. Chem. C*, 2023, **11**, 593–599

This journal is © The Royal Society of Chemistry 2023

The long-term stability of 2D material based devices under ambient conditions has often been a point of debate. Grown $PtSe_2$ films are known to be stable under ambient conditions, however exfoliated films have never been investigated. Thus, we compare the performance of a sensor after it has been in N_2 flow storage for 15 months. The film conductance surprisingly increased slightly as shown in Fig. 3a. The improved conductivity after 15 months of storage could be due to the formation of better intersheet contacts or residual water in the film acting as a p-dopant increasing the concentration of majority charge carriers. During NH_3 gas sensing, interestingly, the peak-to-peak value of relative resistance changes slightly as the initial resistance decreased after 15 months, but the device exhibits higher SNR values because the RMS noise decreased. Fig. 3d presents the sensor response upon decreasing the NH_3 introduction time from 60 to 10 seconds in the same period, indicating that the estimated detection limit exponentially increases from 0.059 to 0.721 ppm (inset).

In conclusion, the devices still function as a very sensitive ammonia sensor after 15 months of storage. This is a remarkable finding as the long-term stability of LPE derived devices has always been a point of discussion while the high stability $PtSe_2$ has been so far only reported for thermally-assisted conversion (TAC) derived films.[11]

Conclusions

The formation of LB-type films into tiled networks from LPE-$PtSe_2$ dispersions was achieved for the first time. This combination resembles a cornerstone for a high yield, scalable, low cost production of sensors. This method is suitable for highly sought after flexible and wearable devices. We characterized the tiled network films structurally and revealed homogeneous films with little roughness indicating good alignment of the $PtSe_2$ flakes. We showed ~ 7.6 times higher conductivity in the tiled nanosheet network films through the modified LB production method in comparison to the conventional spray-deposited films. Thus, this method allows deposition to much thinner conducting networks forming 2D materials. The sensor performance of the LPE-$PtSe_2$ LB films showed high sensitivity toward NH_3 down to 0.100 ppm, which is remarkably low compared to those of most other 2D material based gas sensors. Furthermore, we demonstrated the long-term stability of the $PtSe_2$ based sensor over more than one year.

Author contributions

K. L.: data curation, formal analysis, investigation, validation, visualization, writing – original draft, and writing – review & editing; B. M. S.: conceptualization, data curation, investigation, methodology, and writing – original draft; O. H.: formal analysis, investigation, and visualization; K. S.: data curation, formal analysis, and investigation, B. T.: investigation; T. H.: investigation; T. T.: investigation, methodology, visualization, and writing – review & editing; C. P. G.: formal analysis and investigation;

J. N. C.: funding acquisition, and resources; Z. S.: funding acquisition and resources; M. S.: conceptualization, funding acquisition, methodology, supervision, and writing – review & editing; C. B.: conceptualization, funding acquisition, methodology, resources, visualization, supervision, and writing – review & editing; G. S. D.: funding acquisition, project administration, supervision, and writing – review & editing.

Conflicts of interest

There are no conflicts to declare.

Acknowledgements

Notes and references

1 A. K. Geim and K. S. S. Novoselov, *Nat. Mater.*, 2007, **6**, 183–191.

2 H. Schmidt, F. Giustiniano and G. Eda, *Chem. Soc. Rev.*, 2015, **44**, 7715–7736.

3 C. Backes, A. M. Abdelkader, C. Alonso, A. Andrieux-Ledier, R. Arenal, J. Azpeitia, N. Balakrishnan, L. Banszerus, J. Barjon, R. Bartali, S. Bellani, C. Berger, R. Berger, M. M. B. Ortega, C. Bernard, P. H. Beton, A. Beyer, A. Bianco, P. Bøggild, F. Bonaccorso, G. B. Barin, C. Botas, R. A. Bueno, D. Carriazo, A. Castellanos-Gomez, M. Christian, A. Ciesielski, T. Ciuk, M. T. Cole, J. Coleman, C. Coletti, L. Crema, H. Cun, D. Dasler, D. De Fazio, N. Díez, S. Drieschner, G. S. Duesberg, R. Fasel, X. Feng, A. Fina, S. Forti, C. Galiotis, G. Garberoglio, J. M. García, J. A. Garrido, M. Gibertini, A. Gölzhäuser, J. Gómez, T. Greber, F. Hauke, A. Hemmi, I. Hernandez-Rodriguez, A. Hirsch, S. A. Hodge, Y. Huttel, P. U. Jepsen, I. Jimenez, U. Kaiser, T. Kaplas, H. Kim, A. Kis, K. Papagelis, K. Kostarelos, A. Krajewska, K. Lee, C. Li, H. Lipsanen, A. Liscio, M. R. Lohe, A. Loiseau, L. Lombardi, M. Francisca López, O. Martin, C. Martín, L. Martínez, J. A. Martin-Gago, J. Ignacio Martínez, N. Marzari, Á. Mayoral, J. McManus, M. Melucci, J. Méndez, C. Merino, P. Merino, A. P. Meyer, E. Miniussi,

This journal is © The Royal Society of Chemistry 2023

J. Mater. Chem. C, 2023, **11**, 593–599 | **597**

V. Miseikis, N. Mishra, V. Morandi, C. Munuera, R. Muñoz, H. Nolan, L. Ortolani, A. K. Ott, I. Palacio, V. Palermo, J. Parthenios, I. Pasternak, A. Patane, M. Prato, H. Prevost, V. Prudkovskiy, N. Pugno, T. Rojo, A. Rossi, P. Ruffieux, P. Samorì, L. Schué, E. Setijadi, T. Seyller, G. Speranza, C. Stampfer, I. Stenger, W. Strupinski, Y. Svirko, S. Taioli, K. B. K. Teo, M. Testi, F. Tomarchio, M. Tortello, E. Treossi, A. Turchanin, E. Vazquez, E. Villaro, P. R. Whelan, Z. Xia, R. Yakimova, S. Yang, G. R. Yazdi, C. Yim, D. Yoon, X. Zhang, X. Zhuang, L. Colombo, A. C. Ferrari and M. Garcia-Hernandez, *2D Mater.*, 2020, **7**, 022001.

4 F. Schedin, A. K. Geim, S. V. Morozov, E. W. Hill, P. Blake, M. I. Katsnelson and K. S. Novoselov, *Nat. Mater.*, 2007, **6**, 652–655.

5 H. Li, Z. Yin, Q. He, H. Li, X. Huang, G. Lu, D. W. H. Fam, A. I. Y. Tok, Q. Zhang and H. Zhang, *Small*, 2012, **8**, 63–67.

6 D. J. Late, Y. K. Huang, B. Liu, J. Acharya, S. N. Shirodkar, J. Luo, A. Yan, D. Charles, U. V. Waghmare, V. P. Dravid and C. N. R. Rao, *ACS Nano*, 2013, **7**, 4879–4891.

7 K. Lee, R. Gatensby, N. McEvoy, T. Hallam and G. S. Duesberg, *Adv. Mater.*, 2013, **25**, 6699–6702.

8 H. Fang, S. Chuang, T. C. Chang, K. Takei, T. Takahashi and A. Javey, *Nano Lett.*, 2012, **12**, 3788–3792.

9 M. O'Brien, K. Lee, R. Morrish, N. C. Berner, N. McEvoy, C. A. Wolden and G. S. Duesberg, *Chem. Phys. Lett.*, 2014, **615**, 6–10.

10 D. J. Late, T. Doneux and M. Bougouma, *Appl. Phys. Lett.*, 2014, **105**, 233103.

11 C. Yim, K. Lee, N. McEvoy, M. O'Brien, S. Riazimehr, N. C. Berner, C. P. Cullen, J. Kotakoski, J. C. Meyer, M. C. Lemme and G. S. Duesberg, *ACS Nano*, 2016, **10**, 9550–9558.

12 L. Pi, L. Li, K. Liu, Q. Zhang, H. Li and T. Zhai, *Adv. Funct. Mater.*, 2019, **1904932**, 1904932.

13 X. Chen, C. Liu and S. Mao, *Nano-Micro Lett.*, 2020, **12**, 95.

14 M. Sajjad, E. Montes, N. Singh and U. Schwingenschlögl, *Adv. Mater. Interfaces*, 2017, **4**, 1600911.

15 X. Chia, A. Adriano, P. Lazar, Z. Sofer, J. Luxa and M. Pumera, *Adv. Funct. Mater.*, 2016, **26**, 4306–4318.

16 N. Rohaizad, C. C. Mayorga-Martinez, Z. Sofer, R. D. Webster and M. Pumera, *Appl. Mater. Today*, 2020, **19**, 100606.

17 Y. Hernandez, V. Nicolosi, M. Lotya, F. M. Blighe, Z. Sun, S. De, I. T. McGovern, B. Holland, M. Byrne, Y. K. Gun'Ko, J. J. Boland, P. Niraj, G. Duesberg, S. Krishnamurthy, R. Goodhue, J. Hutchison, V. Scardaci, A. C. Ferrari and J. N. Coleman, *Nat. Nanotechnol.*, 2008, **3**, 563–568.

18 A. B. Bourlinos, V. Georgakilas, R. Zboril, T. A. Steriotis and A. K. Stubos, *Small*, 2009, **5**, 1841–1845.

19 M. Lotya, Y. Hernandez, P. J. King, R. J. Smith, V. Nicolosi, L. S. Karlsson, F. M. Blighe, S. De, Z. Wang, I. T. McGovern, G. S. Duesberg and J. N. Coleman, *J. Am. Chem. Soc.*, 2009, **131**, 3611–3620.

20 Y. T. Liang and M. C. Hersam, *J. Am. Chem. Soc.*, 2010, **132**, 17661–17663.

21 K. R. Paton, E. Varrla, C. Backes, R. J. Smith, U. Khan, A. O'Neill, C. Boland, M. Lotya, O. M. Istrate, P. King, T. Higgins, S. Barwich, P. May, P. Puczkarski, I. Ahmed, M. Moebius, H. Pettersson, E. Long, J. Coelho, S. E. O'Brien, E. K. McGuire, B. M. Sanchez, G. S. Duesberg, N. McEvoy, T. J. Pennycook, C. Downing, A. Crossley, V. Nicolosi and J. N. Coleman, *Nat. Mater.*, 2014, **13**, 624–630.

22 T. J. Nacken, C. Damm, J. Walter, A. Rüger and W. Peukert, *RSC Adv.*, 2015, **5**, 57328–57338.

23 C. Zhi, Y. Bando, C. Tang, H. Kuwahara and D. Golberg, *Adv. Mater.*, 2009, **21**, 2889–2893.

24 J. N. Coleman, M. Lotya, A. O'Neill, S. D. Bergin, P. J. King, U. Khan, K. Young, A. Gaucher, S. De, R. J. Smith, I. V. Shvets, S. K. Arora, G. Stanton, H.-Y. Kim, K. Lee, G. T. Kim, G. S. Duesberg, T. Hallam, J. J. Boland, J. J. Wang, J. F. Donegan, J. C. Grunlan, G. Moriarty, A. Shmeliov, R. J. Nicholls, J. M. Perkins, E. M. Grieveson, K. Theuwissen, D. W. McComb, P. D. Nellist and V. Nicolosi, *Science*, 2011, **331**, 568–571.

25 P. Yasaei, B. Kumar, T. Foroozan, C. Wang, M. Asadi, D. Tuschel, J. E. Indacochea, R. F. Klie and A. Salehi-Khojin, *Adv. Mater.*, 2015, **27**, 1887–1892.

26 V. Sresht, A. A. H. Pádua and D. Blankschtein, *ACS Nano*, 2015, **9**, 8255–8268.

27 J. Kang, J. D. Wood, S. A. Wells, J.-H. Lee, X. Liu, K.-S. Chen and M. C. Hersam, *ACS Nano*, 2015, **9**, 3596–3604.

28 J. R. Brent, N. Savjani, E. A. Lewis, S. J. Haigh, D. J. Lewis and P. O'Brien, *Chem. Commun.*, 2014, **50**, 13338–13341.

29 D. Hanlon, C. Backes, E. Doherty, C. S. Cucinotta, N. C. Berner, C. Boland, K. Lee, A. Harvey, P. Lynch, Z. Gholamvand, S. Zhang, K. Wang, G. Moynihan, A. Pokle, Q. M. Ramasse, N. McEvoy, W. J. Blau, J. Wang, G. Abellan, F. Hauke, A. Hirsch, S. Sanvito, D. D. O'Regan, G. S. Duesberg, V. Nicolosi and J. N. Coleman, *Nat. Commun.*, 2015, **6**, 8563.

30 C. Gibaja, D. Rodriguez-San-Miguel, P. Ares, J. Gómez-Herrero, M. Varela, R. Gillen, J. Maultzsch, F. Hauke, A. Hirsch, G. Abellán and F. Zamora, *Angew. Chem., Int. Ed.*, 2016, **55**, 14345–14349.

31 Y. Liu, R. Cheng, L. Liao, H. Zhou, J. Bai, G. Liu, L. Liu, Y. Huang and X. Duan, *Nat. Commun.*, 2011, **2**, 579.

32 R. J. Smith, P. J. King, M. Lotya, C. Wirtz, U. Khan, S. De, A. O'Neill, G. S. Duesberg, J. C. Grunlan, G. Moriarty, J. Chen, J. Wang, A. I. Minett, V. Nicolosi and J. N. Coleman, *Adv. Mater.*, 2011, **23**, 3944–3948.

33 G. S. Bang, K. W. Nam, J. Y. Kim, J. Shin, J. W. Choi and S.-Y. Choi, *ACS Appl. Mater. Interfaces*, 2014, **6**, 7084–7089.

34 E. Varrla, C. Backes, K. R. Paton, A. Harvey, Z. Gholamvand, J. McCauley and J. N. Coleman, *Chem. Mater.*, 2015, **27**, 1129–1139.

35 Y. Liu, X. Ji, J. Liu, W. W. L. Tong, D. Askhatova and J. Shi, *Adv. Funct. Mater.*, 2017, **27**, 1703261.

36 J. Kang, V. K. Sangwan, J. D. Wood, X. Liu, I. Balla, D. Lam and M. C. Hersam, *Nano Lett.*, 2016, **16**, 7216–7223.

37 P. Schiettecatte, A. Rousaki, P. Vandenabeele, P. Geiregat and Z. Hens, *Langmuir*, 2020, **36**, 15493–15500.

38 E. Petroni, E. Lago, S. Bellani, D. W. Boukhvalov, A. Politano, B. Gürbulak, S. Duman, M. Prato, S. Gentiluomo, R. Oropesa-Nuñez, J.-K. Panda, P. S. Toth, A. E. Del Rio Castillo, V. Pellegrini and F. Bonaccorso, *Small*, 2018, **14**, 1800749.

598 | *J. Mater. Chem. C*, 2023, **11**, 593–599

This journal is © The Royal Society of Chemistry 2023

39 M. M. Y. A. Alsaif, S. Balendhran, M. R. Field, K. Latham, W. Wlodarski, J. Z. Ou and K. Kalantar-zadeh, *Sens. Actuators, B*, 2014, **192**, 196–204.

40 D. Hanlon, C. Backes, T. M. Higgins, M. Hughes, A. O'Neill, P. King, N. McEvoy, G. S. Duesberg, B. Mendoza Sanchez, H. Pettersson, V. Nicolosi and J. N. Coleman, *Chem. Mater.*, 2014, **26**, 1751–1763.

41 Y. Wang, Y.-Z. Zhang, D. Dubbink and J. E. ten Elshof, *Nano Energy*, 2018, **49**, 481–488.

42 J. A. Carrasco, A. Harvey, D. Hanlon, V. Lloret, D. McAteer, R. Sanchis-Gual, A. Hirsch, F. Hauke, G. Abellán, J. N. Coleman and E. Coronado, *Chem. Commun.*, 2019, **55**, 3315–3318.

43 A. J. Molina-Mendoza, E. Giovanelli, W. S. Paz, M. A. Niño, J. O. Island, C. Evangeli, L. Aballe, M. Foerster, H. S. J. van der Zant, G. Rubio-Bollinger, N. Agraït, J. J. Palacios, E. M. Pérez and A. Castellanos-Gomez, *Nat. Commun.*, 2017, **8**, 14409.

44 Y. Niu, J. Villalva, R. Frisenda, G. Sanchez-Santolino, L. Ruiz-González, E. M. Pérez, M. García-Hernández, E. Burzurí and A. Castellanos-Gomez, *2D Mater.*, 2019, **6**, 035023.

45 M. Naguib, O. Mashtalir, J. Carle, V. Presser, J. Lu, L. Hultman, Y. Gogotsi and M. W. Barsoum, *ACS Nano*, 2012, **6**, 1322–1331.

46 R. Z. Lange, K. Synnatschke, H. Qi, N. Huber, G. Hofer, B. Liang, C. Huck, A. Pucci, U. Kaiser, C. Backes and A. D. Schlüter, *Angew. Chem., Int. Ed.*, 2020, **59**, 5683–5695.

47 A. Harvey, C. Backes, Z. Gholamvand, D. Hanlon, D. McAteer, H. C. Nerl, E. McGuire, A. Seral-Ascaso, Q. M. Ramasse, N. McEvoy, S. Winters, N. C. Berner, D. McCloskey, J. F. Donegan, G. S. Duesberg, V. Nicolosi and J. N. Coleman, *Chem. Mater.*, 2015, **27**, 3483–3493.

48 C. Backes, B. M. Szydłowska, A. Harvey, S. Yuan, V. Vega-Mayoral, B. R. Davies, P. L. Zhao, D. Hanlon, E. J. G. Santos, M. I. Katsnelson, W. J. Blau, C. Gadermaier and J. N. Coleman, *ACS Nano*, 2016, **10**, 1589–1601.

49 B. M. Szydłowska, O. Hartwig, B. Tywoniuk, T. Hartman, T. Stimpel-Lindner, Z. Sofer, N. McEvoy, G. S. Duesberg and C. Backes, *2D Mater.*, 2020, **7**, 045027.

50 X. Li, G. Zhang, X. Bai, X. Sun, E. Wang and H. Dai, *Nat. Nanotechnol.*, 2008, **3**, 538–542.

51 L. J. Cote, F. Kim and J. Huang, *J. Am. Chem. Soc.*, 2009, **131**, 1043–1049.

52 H. Kim, C. Mattevi, H. J. Kim, A. Mittal, K. A. Mkhoyan, R. E. Riman and M. Chhowalla, *Nanoscale*, 2013, **5**, 12365.

53 T. Tomašević-Ilić, J. Pešić, I. Milošević, J. Vujin, A. Matković, M. Spasenović and R. Gajić, *Opt. Quantum Electron.*, 2016, **48**, 319.

54 S. Andrić, M. Sarajlić, M. Frantlović, I. Jokić, D. Vasiljević-Radović and M. Spasenović, *Chemosensors*, 2021, **9**, 342.

55 P. Blake, P. D. Brimicombe, R. R. Nair, T. J. Booth, D. Jiang, F. Schedin, L. A. Ponomarenko, S. V. Morozov, H. F. Gleeson, E. W. Hill, A. K. Geim and K. S. Novoselov, *Nano Lett.*, 2008, **8**, 1704–1708.

56 F. Torrisi, T. Hasan, W. Wu, Z. Sun, A. Lombardo, T. S. Kulmala, G.-W. Hsieh, S. Jung, F. Bonaccorso, P. J. Paul, D. Chu and A. C. Ferrari, *ACS Nano*, 2012, **6**, 2992–3006.

57 T. Tomašević-Ilić, Đ. Jovanović, I. Popov, R. Fandan, J. Pedrós, M. Spasenović and R. Gajić, *Appl. Surf. Sci.*, 2018, **458**, 446–453.

58 F. Reincke, S. G. Hickey, W. K. Kegel and D. Vanmaekelbergh, *Angew. Chem., Int. Ed.*, 2004, **43**, 458–462.

59 H. Duan, D. Wang, D. G. Kurth and H. Möhwald, *Angew. Chem., Int. Ed.*, 2004, **43**, 5639–5642.

60 A. G. Kelly, D. O'Suilleabhain, C. Gabbett and J. N. Coleman, *Nat. Rev. Mater.*, 2021, **7(3)**, 217–234.

61 J. Wu, H. Li, Z. Yin, H. Li, J. Liu, X. Cao, Q. Zhang and H. Zhang, *Small*, 2013, **9**, 3314–3319.

62 A. Matković, I. Milošević, M. Milićević, T. Tomašević-Ilić, J. Pešić, M. Musić, M. Spasenović, D. Jovanović, B. Vasić, C. Deeks, R. Panajotović, M. R. Belić and R. Gajić, *2D Mater.*, 2016, **3**, 015002.

63 Y.-J. Li, W.-J. Huang and S.-G. Sun, *Angew. Chem., Int. Ed.*, 2006, **45**, 2537–2539.

64 C. Backes, D. Campi, B. M. Szydlowska, K. Synnatschke, E. Ojala, F. Rashvand, A. Harvey, A. Griffin, Z. Sofer, N. Marzari, J. N. Coleman and D. D. O'Regan, *ACS Nano*, 2019, **13**, 7050–7061.

65 Y. Zhao, J. Qiao, Z. Yu, P. Yu, K. Xu, S. P. Lau, W. Zhou, Z. Liu, X. Wang, W. Ji and Y. Chai, *Adv. Mater.*, 2017, **29**, 1604230.

66 C. Yim, V. Passi, M. C. Lemme, G. S. Duesberg, C. Ó. Coileáin, E. Pallecchi, D. Fadil and N. McEvoy, *npj 2D Mater. Appl.*, 2018, **2**, 5.

67 T. Das, E. Yang, J. E. Seo, J. H. Kim, E. Park, M. Kim, D. Seo, J. Y. Kwak and J. Chang, *ACS Appl. Mater. Interfaces*, 2021, **13(1)**, 1861–1871.

68 G. Eda and M. Chhowalla, *Nano Lett.*, 2009, **9**, 814–818.

69 Q. Zheng, W. H. Ip, X. Lin, N. Yousefi, K. K. Yeung, Z. Li and J. K. Kim, *ACS Nano*, 2011, **5**, 6039–6051.

70 Q. Li, Q. Zhou, L. Shi, Q. Chen and J. Wang, *J. Mater. Chem. A*, 2019, **7**, 4291–4312.

71 J. Li, Y. Lu, Q. Ye, M. Cinke, J. Han and M. Meyyappan, *Nano Lett.*, 2003, **3**, 929–933.

72 L. A. Currie, *Pure Appl. Chem.*, 1995, **67**, 1699–1723.

73 O. Leenaerts, B. Partoens and F. Peeters, *Phys. Rev. B: Condens. Matter Mater. Phys.*, 2008, **77**, 125416.

74 S. Zhao, J. Xue and W. Kang, *Chem. Phys. Lett.*, 2014, **595–596**, 35–42.

This journal is © The Royal Society of Chemistry 2023

J. Mater. Chem. C, 2023, **11**, 593–599 | **599**